J Fail. Anal. and Preven. (2024) 24:559–574
https://doi.org/10.1007/s11668-024-01858-1

ORIGINAL RESEARCH ARTICLE

Microstructure-Based Creep Life Assessment of 1CrMoV Turbine Rotor Steels After Long-Term Service

Hlanganani Siphelele Nyembe · Philip van der Meer · Robert Knutsen · Johan Ewald Westraadt

Submitted: 12 December 2023 / Accepted: 2 January 2024 / Published online: 6 February 2024
© The Author(s) 2024

Abstract This study evaluates the use of quantitative analytical electron microscopy for microstructure-based creep life assessment of service-exposed 1CrMoV steel turbine rotors. Changes in the microstructure (bainitic laths, carbide phases) were related to creep life exhaustion estimations done using conventional methods based on cavities and hardness. The volume-weighted average size and surface density of bainitic laths correlate with cavity-based estimated creep life exhaustion. However, the heterogeneity of grain structure limits the use of bainitic lath parameters for assessing creep life based on microstructure. The phase proportions of M_3C, M_2C, and M_7C_3 carbides, as determined by TKD-EDS mapping, show a strong correlation (R^2: 0.64, 0.61, and 0.86) with creep life exhaustion estimations and could potentially be used as an additional indicator of the material state of the critical failure region in 1CrMoV turbine rotors.

Keywords Microstructure · Electron microscopy · Creep life exhaustion · Long-term service · 1CrMoV steel rotor

H. S. Nyembe (✉) · J. E. Westraadt
Department of Physics, Centre for HRTEM, Nelson Mandela University, Gqeberha, South Africa
e-mail: nyembehs@gmail.com

P. van der Meer · R. Knutsen
Department of Mechanical Engineering, Centre for Materials Engineering, University of Cape Town, Cape Town, South Africa

R. Knutsen
Electron Microscope Unit, University of Cape Town, Cape Town, South Africa

Introduction

The electrical power generating industry is currently dominated by fossil fuel-based technologies. Increasing regulations and the transition to competitive cleaner and renewable technologies are big driving forces for the replacement of these fossil fuel technologies. In the interim, the current economic climate does not always allow for wholesale upgrades to aging components on fossil fuel-based plants with a limited operating span, since the payback period might not be realized. This means that existing infrastructures might need to be operated for extended periods until these newer technologies come online. Due to variations in service operating conditions, material properties due to non-optimal manufacturing processes, chemical composition, or non-optimal installation procedures, critical high-temperature/high-pressure components could be at an increased risk for catastrophic failures when components are operated for extended periods [1]. It is critical to manage these costly high-risk plant components in a safe but economical manner.

One tool to assess the integrity of high-temperature and high-pressure components is surface replication. This nondestructive technique is used extensively to classify the material damage category of a component. The number of voids per mm^2 in an acetate replica film is manually counted with an optical microscope and used in conjunction with conservative remnant life models to manage the inspection frequency and replacement of power plant components [2, 3]. In cases where the surface is inaccessible or the component damage is below the surface, then specialized sampling technologies are required to remove material from the plant component [4]. This allowed for an improved life assessment of the rotors and ensuring reliable

service extension. However, conventional life assessment methods are applied on a conservative basis, which leads to the premature retirement of the rotor.

Creep resistant 1CrMoV steels are used extensively for high-pressure (HP) turbine rotors operated at steam temperatures up to approximately 565 °C. These steels have the microstructure that provides a combination of high creep strength and good toughness properties. The HP turbine rotors operate in temperatures and stresses, where creep is a concern for 1CrMoV steels. Creep is the primary damage mechanism limiting the life of 1CrMoV rotors. Creep causes the microstructure of the rotors to change extremely slowly during the long-term service. Monitoring microstructural changes is a potential way to assess loss of creep strength and creep life exhaustion. Any technique that accurately measures the creep history of the rotor during service can save costs by providing precise life assessments. Therefore, life assessment of the rotors based on in-service microstructural degradation is crucial in ensuring safe and cost-effective operation [1, 2].

The microstructure of 1CrMoV rotors comprises packets of elongated and polygonal bainitic laths within prior austenite grains (PAGs), high dislocation density in the bainitic ferrite matrix, and dispersion of alloy carbides in the grain boundaries and within ferrite matrix [5]. The microstructure and creep properties of 1CrMoV rotors degrade during service under creep conditions. The in-service microstructural degradation includes recovery of dislocations and bainitic lath structure, coarsening of carbides, formation of new carbides, enrichment of alloying elements in carbides, and depletion of alloying elements in matrix [6–8]. These microstructural changes are interrelated and contribute to the reduction of hardness and formation of creep cavities or voids. Creep failure occurs by creep cavity-induced intergranular (cavitation) fracture in 1CrMoV steel rotors [9]. Bhadeshia et al. [10] reviewed methods which exploit the changes in microstructure, hardness, and cavities for RLA of ferritic power plant steels. The hardness and creep cavities have been extensively used for life assessment of low-alloy steel components [11].

Creep Life Assessment

Hardness measurements can be used to estimate the extent of creep life exhaustion undergone by a material exposed to creep conditions for a long time. The hardness of 1CrMoV steel rotors after heat treatment is in the range of 240–260 HV [9, 12–14]. The hardness of 1CrMoV rotor decreases after the incubation time of 100 kh during service exposure at temperatures above 450 °C [6, 8, 12, 15]. Goto [16] (as cited in references [1, 10–12]) correlated the hardness reduction for various service-exposed 1CrMoV rotors with service exposure time (t), temperature (T) and stress (σ). This relationship has been used to estimate the effective metal temperature (T_e) [2] and creep life exhaustion [12] for service-exposed 1CrMoV rotors. Cardoso et al. [12] presented an overall procedure for RLA of service-exposed 1CrMoV rotor based on hardness measurements. The normalized hardness and fractional creep life exhaustion (t/t_r) are related by an empirical relationship as mentioned in Eq 1 [10, 16]. The normalized hardness is the ratio between the hardness of the initial material (H_0) and crept material (H_t). This empirical relationship applies during secondary creep regime before the onset of gross damage. During tertiary creep, the crept materials with the same H_t can have different t/t_r values [17].

The blade attachment grooves in 1CrMoV turbine rotors are subject to high stresses which results in the development of creep cavities in service-exposed 1CrMoV rotors [1, 11]. The creep cavitation is the precursor to the creep crack initiation that ultimately results in creep failure. There are various models describing the variation of cavity density and diameter [3], A-parameter and area fraction [19], and length [20] with the creep life for accelerated creep tested 1CrMoV steels. Van Zyl et al. [3] and van der Meer et al. [2] presented the procedure for RLA, which uses number density of creep voids to predict t/t_r on 1CrMoV rotors operating for over 100 kh. The fractional creep life exhaustion is correlated with the cavity density fraction (N_t/N_f) as mentioned in Eq 2, where operating time is t (h), crack initiation time is t_r (h), cavity density after service is N_t (mm^{-2}), cavity density at fracture is N_f (mm^{-2}), and material creep ductility parameter is λ. This model is extensively used in the evaluation of t/t_r of high-temperature steel components. However, the main limitation with this model is the estimation of λ because λ determined at a low creep life exhaustion may not be descriptive of the situation at a higher creep life exhaustion [3, 21].

$$\frac{H_t}{H_0} = 1 - 5500\,\frac{t}{t_r}\,e^{\frac{-8511}{T}} \qquad \text{(Eq 1)}$$

$$\frac{t}{t_r} = 1 - \left(1 - \frac{N_t}{N_f}\right)^{\lambda} \qquad \text{(Eq 2)}$$

In-Service Microstructural Degradation

Typical heat treatment of 1CrMoV steel rotors comprises austenitization at 950 °C, quenching, and tempering between 690 and 710 °C. Studies are available that discuss the microstructure of low-alloy 1CrMoV steel rotors in the pre-service condition [9, 11, 22–26]. The microstructural investigations of 1CrMoV rotors in the pre-service condition reveal the distribution of M_3C (M = Fe, Cr, Mn), MC or M_4C_3 (M = V, Mo, Cr), and M_2C (M = Mo, V, Cr) carbides. Coarse M_3C precipitates exist as the principal

carbide phase, while fine M_2C platelets and MC spherical precipitates exist as the minority phases. The M_3C carbides grow on grain boundaries, while MC and M_2C carbides precipitate on grain boundaries and dislocations within the ferrite matrix [7–9, 23–26]. These carbides hinder the dislocation movement [27]. Senior [26] reviews six types of carbides which form in 1CrMoV steel: M_3C, MC, M_2C, M_7C_3 (M = Cr, Fe, Mn), $M_{23}C_6$ (M = Fe, Cr, Mn), and M_6C (M = Mo, Fe).

Many studies are available that discuss the microstructure of 1CrMoV steel rotors subjected to *accelerated* creep testing [9, 24–26] and service exposure [7, 8, 26]. The microstructure of low-alloy CrMoV steels subjected to thermal aging or accelerated creep testing at temperatures above 600 °C is discussed in [26–35]. Microstructural investigations of ferritic CrMoV steel power plant components subjected to *long-term* service exposure at temperatures below 565 °C are presented in references [7, 8, 36–42]. The major microstructure degradation of 1CrMoV rotors caused by creep during service or accelerated creep testing can be classified into:

1. Coarsening of M_3C, MC, and M_2C precipitates [7, 8, 26].
2. Enrichment of Cr and Mn in M_3C carbides [8].
3. Enhanced secondary precipitation of M_2C precipitates [7].
4. Dissolution of M_3C carbides, secondary precipitation and coarsening of $M_{23}C_6$ and M_7C_3 carbides on grain boundaries [7, 8].
5. Depletion of Cr, Mo, and V in ferrite matrix [7, 8].
6. Recovery of dislocations within the bainitic ferrite matrix [9, 24, 25].
7. Coarsening of bainitic laths [9, 24, 25].
8. Cavitations at grain boundaries [2, 9, 20, 43].

Microstructural Characterization

Microstructural investigations of CrMoV steels have been mainly performed using optical microscopy (OM), scanning electron microscopy (SEM), transmission electron microscopy (TEM), energy-dispersive X-ray spectroscopy (EDX), and X-ray diffraction (XRD)-based techniques. These methods have different advantages and limitations in terms of sample preparation, field of view, and data analysis complexity. Therefore, selecting the appropriate method is crucial for obtaining representative microstructural data in a reasonable amount of time. Investigations of bainitic laths, PAGs, carbide precipitates, and cavities in CrMoV steels have been mainly performed on the polished or etched cross-sectional area of bulk samples using OM [6, 8, 27–29, 38, 44–46] and SEM [24, 28, 35–37, 39, 40, 43–48] techniques. To reveal PAGs, grain boundary segregation, carbides, and cavities, etching is performed using solutions of Nital [8, 30, 38], picric acid [44, 46], and Vilella [28]. The SEM offers enhanced resolution, which enables the examination of nano-sized cavities and carbides. The chemical analysis of carbides has been done on etched bulk sample surfaces using EDX in the SEM [24, 30, 39]. Ohtani et al. [25] studied the bainitic laths, misorientations, and dislocations on the polished *bulk samples* of 1CrMoV rotor steel using the SEM-based electron backscattered diffraction (EBSD) technique.

A combination of *thin foil*, scanning transmission electron microscopy (STEM), selected area electron diffraction (SAED), and energy-dispersive X-ray spectroscopy (EDX) has been used to study bainitic structure, dislocations within bainitic ferrite, carbide precipitates, and chemical composition in CrMoV steels [7, 9, 23–25, 28, 29, 32, 35, 37–39, 42, 45, 46]. Shinya et al. [9] used *thin foils* to study dislocations within the bainitic ferrite with X-ray diffraction (XRD) on 1CrMoV rotor steel. The main advantage of *thin foils* is that the precipitate nucleation site is preserved and the spatial resolution in the TEM is sufficient to resolve the very fine precipitates. It is difficult to examine fine precipitates in *bulk samples* and *thin foil*s without obtaining a strong matrix signal. To avoid matrix interference, investigations of carbide precipitates on CrMoV steels have been performed on *extraction replicas* using STEM, SAED, and EDX [8, 27, 29–31, 34, 37, 38, 44, 46]. Mitchell and Moss [8] and Wang et al. [49] briefly discusses STEM-EDX examination of carbide precipitates on *extraction replicas* obtained from 1CrMoV steel rotors and 12Cr1MoV steel, respectively. Westraadt et al. [50] studied precipitates on *extraction replicas* obtained from 12Cr1MoV steel using transmission Kikuchi diffraction (TKD) in the SEM. The major limitation of the *extraction replicas* in 1CrMoV steel rotors is the uncertainty in the extraction efficiency of carbides caused by variable etching response of the various rotors [8]. A detailed TKD analysis of nano-precipitates on extraction replicas is presented in the work of Bhattacharya et al. [51]. XRD analysis of carbides phases has been performed on carbides isolated from the Fe matrix by electrolytic extraction technique [27, 30, 32, 34, 35, 46].

Limited research has been done on the highly stressed regions in the blade attachment area of 1CrMoV steel rotors. The objective of this study is to evaluate the use of quantitative electron microscopy as a *microstructure-based* life assessment tool for 1CrMoV rotor steels which have been subject to long-term service (270–300 kh). The study reports on the application of a wide range of quantitative electron microscopy techniques to characterize the microstructural features in service-exposed 1CrMoV steel turbine rotor and how these features correlate with

fractional creep life exhaustion estimated based on hardness and cavitation. The current study discusses the advantages and limitations of using electron microscopy techniques and specific microstructural parameters for life assessment.

Materials and Methods

Materials

Samples were taken from four investigated 1CrMoV steel HP turbine rotors operated for 270–300 kh. The typical chemical composition (%) of the rotors is: 0.27–0.33 C, 0.22–0.4 Si, 0.5–0.72 Mn, 0.011–0.017 P, 0.007–0.017 S, 0.9–1.29 Cr, 0.76–1.23 Mo, 0.51–0.74 Ni, 0.25–0.28 V and (balance) Fe. The chemical composition of the individual rotors is reported elsewhere [51]. The cylindrical core samples were removed from the stage 1 disk of the HP turbine rotors. The position of the core sample was chosen to include the highest creep-damaged area on the rotor. In rotor 1, two core samples (H3 and H4) separated by 180° in the blade groove were removed to study the heterogeneity. The core samples were removed using the Weldcore® technology, as described by Doubell et al. [4]. The core samples were sectioned in half to expose the cross-sectional area for the analysis of the bulk and peak stress regions illustrated in Fig. 1. The bulk and peak stress areas of the rotor operate at ~ 538 °C, but the peak stress area experiences higher localized stresses of ~ 70 MPa compared to the bulk (~50–30 MPa) [4]. The core samples were subjected to creep during service and represent the degraded service-exposed (DSE) material state of 1CrMoV steel rotors. During service, the cold section sample was subjected to the temperature of 226 °C where creep is not a concern and represents the initial material (R) state of 1CrMoV steel.

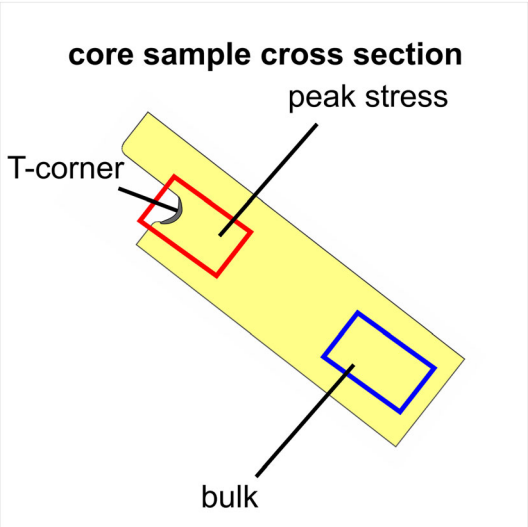

Fig. 1 Schematic diagram for the cross section of the core sample (hot section) shows the peak stress and bulk areas

Microstructural Characterization

Hardness testing was done by indenting samples with a 0.3 kg load using an array of indentations with a uniform spacing of ± 250 µm. Hardness mapping was conducted over ~ 1750 × 1250 µm^2 area to ensure an accurate representation of hardness. The effective metal temperature (T_e) and creep life exhaustion (t/t_r) in the DSE states of the rotors were computed using methods described in references [1, 10–12, 53].

Scanning electron microscopy evaluations were conducted using a JEOL JSM 7001F SEM equipped with an Oxford Instruments® Aztec^{TM} EBSD system and a Nordlys-S^{TM} EBSD detector. BSE and SE characterization of the cross-sectional samples was performed at 15 kV. The quantitative analysis of creep voids was performed using BSE imaging at a resolution of 117 nm/pixel on the polished *cross sections* of the samples. BSE images were collected sequentially with each field of view (FoV) covering 600 × 450 µm^2 area. The collected images were overlapped by ~ 20%, and contrast and brightness were kept constant between the consecutive micrographs to ensure proper merging into a large-BSE image. The images were stitched to generate a single *large-BSE* image with the area up to 4 × 2 mm^2 using ImageJ [17]. The number density (N_t) and equivalent circle diameter (d) of cavities were quantified from the *large-BSE* images using the MIPAR [18] image analysis software. The minimum d of cavities that could be quantified was about 300 nm. However, only cavities with d ~ 1 µm and above were considered for the analysis. The fractional creep life exhausted for the investigated rotors was quantified using the creep cavitation model (Eq 2) described in references [2, 3]. For low-alloy steels which operated for over 150 kh, λ = 3.37 and N_f = 1000 mm^{-2} were applied.

The cross-sectional samples were etched with 2% Nital solution to reveal grain boundaries and carbide precipitates. SE and BSE characterization of the cross-sectional samples in both the polished and etched condition was performed with FoV set to 48 × 36 µm^2, 24 × 18 µm^2 and 12 × 8 µm^2. EBSD characterization was performed on the polished cross-sectional samples using 20 kV accelerating voltage and 70° sample tilt. EBSD measurements were taken at *low magnification* (FoV: 612 × 459 µm^2) and 1 µm step size to examine large PAGs. For fine grain structure, acquisition was conducted at *high magnification* (FoV: 245 × 184 µm^2) and step size: 200 nm in four areas for each region of interest. The bainitic laths, packets, and

PAGs [54, 55] were reconstructed using the grain reconstruction method in MATLAB [56] using the MTEX toolbox [57]. The misorientations of $\geq 2°$ and $\geq 15°$ across the neighboring pair of pixels were considered as lath and packet boundaries, respectively. The volume-weighted average grain size (d_V) and average grain size (d_{mli}), average grain equivalent circle diameter (d_{ec}), and grain surface density (S_V) for laths, packets, and PAGs were computed. The d_V and d_{mli} were computed using the point-sampled intercept length and mean linear intercept methods outlined by Lehto et al. [58].

Carbides were extracted from 1CrMoV rotor cross-sectional samples using extraction replication described by Wang et al. [49], but 4% Nital solution etchant was used in the current study. STEM-EDX and TEM-SAED analysis of extraction replicas were performed using a JEOL JEM 2100 microscope with a LaB_6 electron gun operated at 200 kV. This microscope is fitted with an Oxford X-Max 80 EDS detector in STEM mode. The chemical composition of carbides in the extraction replicas was studied using STEM-EDX. In the software, the predetermined elements were set as Fe, Cr, Mo, Mn, and V, and the ratio standard setting was set to silicon K-series. Large areas of replicas containing many carbide precipitates within a FoV were evaluated using EDX maps. For EDX maps, eight $7.6 \times 5.3\ \mu m^2$ areas were evaluated and their atomic percentages of Fe, Cr, Mo, Mn, and V were determined. The chemical composition of the EDX mapped large area containing various carbides is called *overall carbide* composition. In these areas mapped by EDX, precipitates were examined by spot EDX to determine the atomic percentages of Fe, Cr, Mo, Mn, and V in individual particles. To study the composition of carbides on a statistically significant basis, a minimum of 150 precipitates was examined by spot EDX across eight areas. The common carbide phases in 1CrMoV steel are M_3C, MC, M_2C, M_6C, M_7C_3, and $M_{23}C_6$, and these carbides have a unique composition [26]. Therefore, the carbide phases were identified based on composition, and the average chemical composition for each carbide phase was calculated.

The morphology and crystal structure of carbide precipitates in *extraction replicas* obtained from 1CrMoV rotors were studied using TEM and SAED. Using TEM, a detailed analysis of electron diffraction patterns from carbide precipitates is conventionally used to identify different carbide phases. Because of the complexity of this technique, the crystal structure of only a few precipitates can be identified in a reasonable period by manually solving diffraction patterns. The crystal structures of the precipitates frequently found in thermally aged 1CrMoV steels were identified using SAED. The spot electron diffraction patterns obtained from these phases were manually indexed using JEMS software [59].

Thermodynamic calculations were performed using commercial CALPHAD software ThermoCalc, in combination with the TCFE10 database [60]. The chemical composition of the rotors and phases such as α-Fe, γ-Fe, M_3C, MC, M_2C, M_7C_3, $M_{23}C_6$, and M_6C were considered for the calculations. The phase equilibria and chemical compositions of carbides were predicted and compared with the experimental findings made in the present work.

TKD-EDX characterization was conducted on the *FIB lamellae* and *extraction replicas* prepared from the cross-sectional samples. FIB lamellae were prepared from 4 sites in the peak stress region of rotor 1 (H3) using Ga-ion FIB-SEM. TKD measurements were taken at an accelerating voltage of 30 kV and sample tilt of $-20°$. TKD measurements on FIB lamellae were taken with FoV set to $6 \times 6\ \mu m^2$ and 20 nm step size. For extraction replicas, the total of Four $49 \times 37\ \mu m^2$ (FoV) areas per sample were measured using 50 nm step size. The crystal information files (#ICSD) of ferrite (24963), M_3C (99002), MC (159870), M_2C (77159), M_7C_3 (76799), $M_{23}C_6$ (2837), and M_6C (101138) were used as input to the Aztec software. EDX elemental mapping of Fe, Cr, Mn, Mo, V, Si, and Nb was acquired simultaneously with TKD measurements. The carbide phase maps were reconstructed using MTEX [57], and their equivalent circle diameter (d_A), area fraction (f_A), number density (N_A), and interparticle spacing (λ_A) were measured using MIPAR software [61]. The percentage phase proportions (f_r), the ratio of the f_A of each carbide phase to the sum of f_A of all carbide phases, was calculated.

Results

Various techniques were employed to study the microstructure and hardness of 1CrMoV rotors in the R and DSE states. The effects of creep exposure on microstructure and hardness were studied by comparing the peak stress area in the DSE state with the R state. A comparison was made between peak stress and bulk areas to study the impact of high stresses on microstructure degradation and hardness in the DSE state.

General Microstructure and Creep Life Exhaustion

Figure 2 shows the typical microstructures of 1CrMoV steel rotor as examined by BSE and SE imaging of the cross-sectional samples. In Fig. 2a, the microstructure had a mixture of fine and coarse PAGs comprising polygonal and elongated bainitic laths. The fine H carbides (i.e., M_2C/MC) were distributed within the bainitic ferrite matrix as

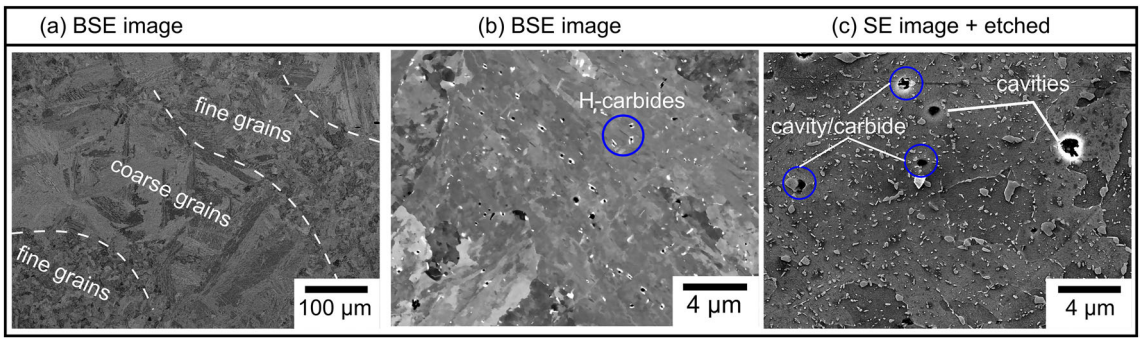

Fig. 2 Typical general microstructure of 1CrMoV steel rotor. (**a**, **b**) BSE images. (**c**) SE images (etched). (**a**) Low magnification (FoV: 600 × 450 µm^2), (**b**, **c**) high magnification (FoV: 24 × 18 µm^2)

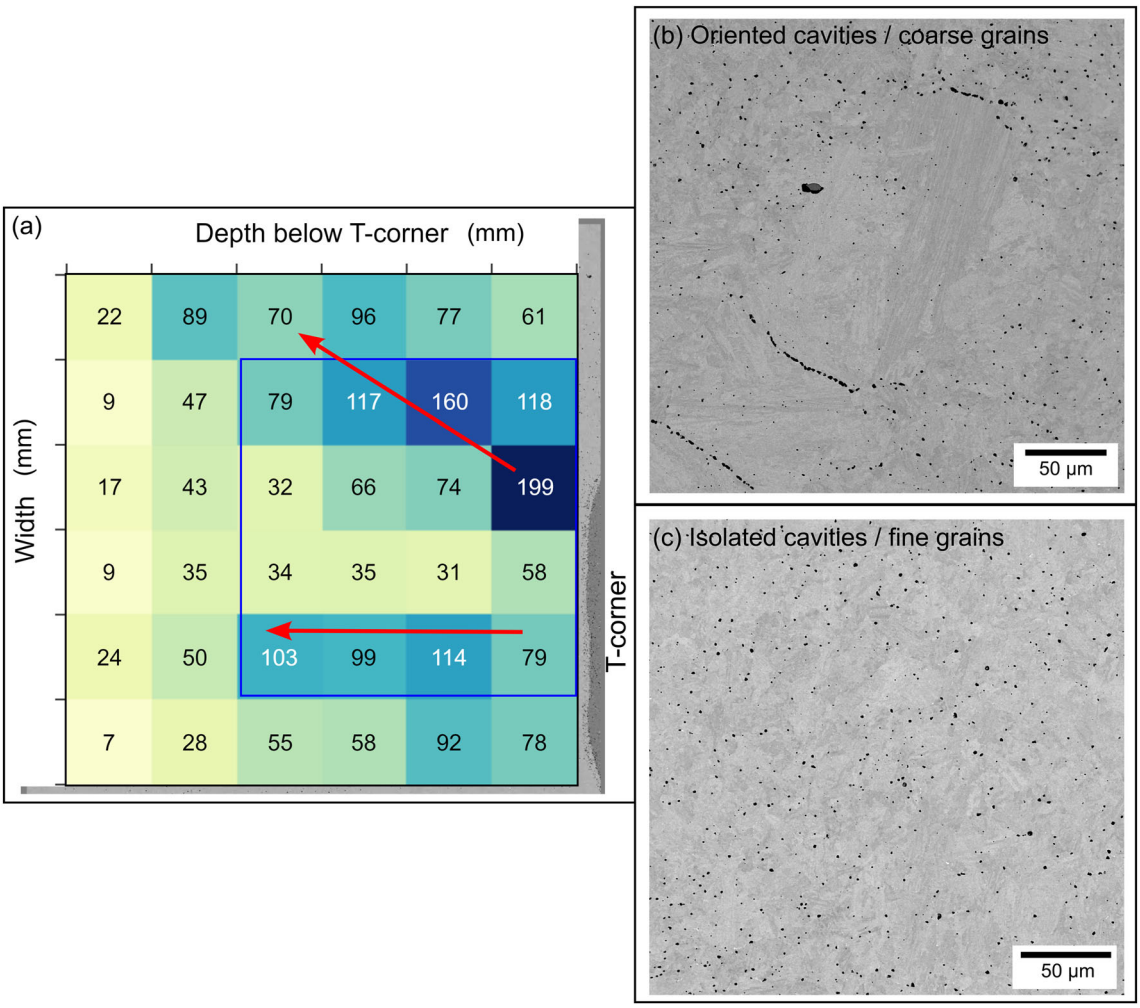

Fig. 3 (**a**) Distribution of number of cavities per 0.25 × 0.25 mm^2 in the peak stress area of rotor 2. BSE images showing cavities around (**b**) coarse and (**c**) fine PAGs

shown in Fig. 2b. SE examination revealed a distribution of coarse carbides on PAG boundaries and fine carbides within PAGs (Fig. 2c). The general microstructure was similar in all material states. However, creep cavities were only observed in the peak stress area in DSE states for all rotors. The distribution of fine and coarse grains was uneven within each sample. In rotor 1 samples H3 and H4, the observable difference in the general microstructure was smaller PAGs in H3 and larger PAGs in H4.

Hardness

The mean hardness values (±*std*-standard deviation) for 1CrMoV steel rotors in the peak stress area are presented in Table 1. The mean hardness in the peak stress area (DSE state) was less than that of the R state. No statistically significant differences were observed between the mean hardness of the *bulk* (not shown) and *peak stress* areas. The normalized hardness (±*sem*-standard error of the mean) and estimated effective metal temperature T_e, and fractional creep life exhaustion (t/t_r) are presented in Table 1. Rotors 2 and 3, with higher T_e, exhibited higher t/t_r than rotors 1 and 4, regardless of operating times. Both H3 and H4 samples from rotor 1 showed similar results for T_e and t/t_r.

Cavitation

BSE examination of the DSE state showed creep cavities only in the peak stress area of all rotors. The number of cavities per 0.25 × 0.25 mm^2 area over the peak stress region of rotor 2 is presented is Fig. 3. In all rotors, creep cavities were dense near the T-corner (marked in Fig. 1) and decreased with depth. The cavities were denser in the regions with fine grains (red arrows) than around coarse grains. Figure 3b and c presents BSE images showing the oriented cavities along coarse grains and isolated cavities around fine grains. The cavity density for the first 1 mm^2 area near the T-corner in the peak stress region (marked by blue lines in Fig. 3a) was considered for creep life calculations. Table 2 presents the cavity density and fractional creep life exhausted (t/t_r) for the rotors. The fractional creep life exhaustion varied between H3 (high density of isolated cavities) and H4 (low density of oriented cavities) in rotor 1.

Table 1 Mean hardness (± *std*) in the peak stress regions, normalized hardness (± *sem*), metal service temperature [16] and fractional creep life exhaustion [10] of the rotors

		t (kh)	H ($HV_{0.3}$)	H/H_0	T_e (°C)	t/t_r
R		0	244 ± 7			
DSE	1 (H3)	288.5	221 ± 4	0.91 ± 0.04	529	0.66
	1 (H4)		222 ± 5	0.91 ± 0.03	529	0.66
	2	272.3	205 ± 5	0.84 ± 0.03	548	0.92
	3	300.4	208 ± 5	0.85 ± 0.03	547	0.88
	4	273.6	222 ± 6	0.91 ± 0.04	530	0.65

Microstructural Analysis

Grains

Figure 4a and b show the example of EBSD orientation maps and grain (lath, PAG) structure of 1CrMoV steel rotors. Large PAGs were split into packets of bainitic laths, while small PAGs had bainitic laths that aligned with PAG. Since 4 areas in each region of interest were studied by EBSD at high magnification, the mean grain d_V, d_{mli}, d_{ec}, and S_V for each area were computed. The mean of means was calculated to represent the average values for each region of interest in the rotor for these size parameters. Table 3 shows the average sizes of lath d_V and PAG d_V, as well as the lath surface density (S_V) in the R and peak stress regions for the rotors in the DSE states. The average PAG d_V was determined using EBSD data collected at low magnification. The lath and PAG sizes (d_V) were significantly smaller in the peak stress of (DSE state) rotors 1 (H3), 2, and 3, as opposed to the R state. However, the lath

Table 2 Cavity density and creep life of rotors

Rotor	1 (H3)	1 (H4)	2	3	4
t (kh)		288.5	272.3	300.4	273.6
N_A (mm^{-2})	345	238	1 398	1 413	195
t/t_r	0.75	0.6	> 1	> 1	0.52

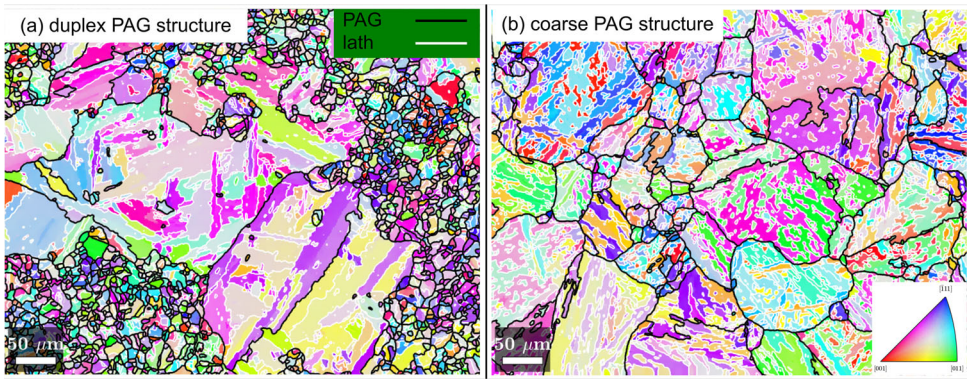

Fig. 4 Typical EBSD orientation maps overlayered with lath and PAG boundaries. (**a**) Mixture of coarse and fine grains. (**b**) coarse grains

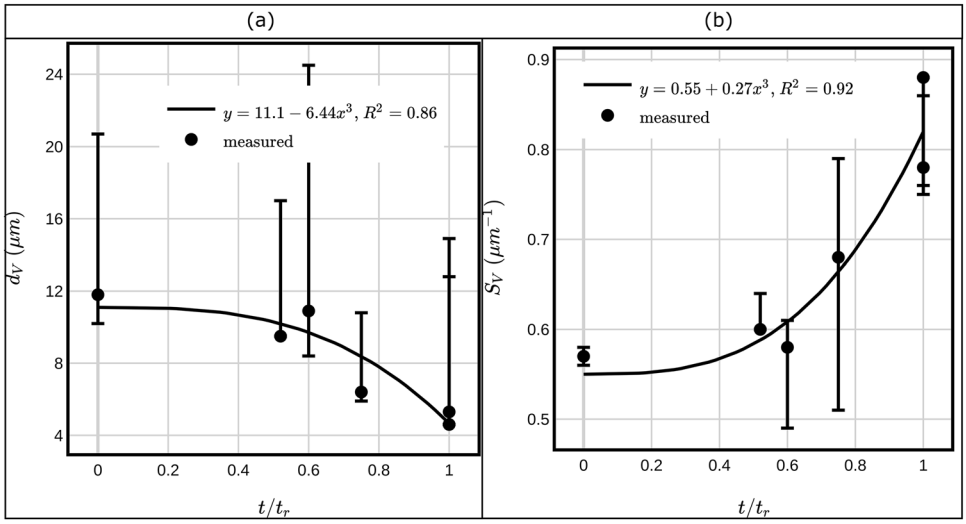

Fig. 5 Variation of the lath (**a**) size d_V and (**b**) surface density S_V (mean of means) with the creep cavitation-based creep life (t/tr). (+error-max mean, -error-min mean)

Table 3 Volume-weighted lath and PAG sizes (d_V) and lath surface density (S_V).

			lath		PAG
		t (kh)	d_V (μm)	S_V (μm^{-1})	d_V (μm)
R		0	12	0.57	62
DSE	1 (H3)	288.5	6	0.70	10
	1 (H4)		12	0.56	71
	2	272.3	5	0.75	14
	3	300.4	5	0.86	14
	4	273.6	10	0.73	69

and PAG sizes (d_V) for rotors 1 (H4) and 4 were similar to the R state. In all rotors except for rotor 1 (H4), the peak stress area exhibited larger lath S_v compared to the R state. In the DSE states of each rotor, the lath and PAG sizes (d_V) for peak stress and bulk areas were comparable. In rotor 1, sample H4 had larger laths and PAG, and lower lath surface density than H3 (Table 3). Creep cavitation in the peak stress regions was also studied from the EBSD data. EBSD revealed that oriented cavities (shown in Fig. 3b) nucleated along PAG–lath boundary intersections. The isolated cavities shown in Fig. 3c nucleated in the PAG–PAG boundary intersections.

Figure 5a and b shows the variation of lath average d_V and S_V with fractional creep life exhausted estimated using the cavitation model for all rotors, respectively. In Fig. 5a, the minus error bar shows the minimum average d_V of the 4 areas examined at high magnification, while the plus error bar represents the average lath d_V of the area examined at low magnification. The positive error bar in Fig. 5b represents the highest S_V of the 4 areas examined at low magnification, whereas the negative error bar represents the lowest S_V. The average lath size decreased in a cubic trend as fractional creep life exhausted increased, as shown in Fig. 5a. However, there is a significant scatter in grain size. In Fig. 5b, the average lath S_V exhibited a cubic trend in relation to fractional creep life exhausted, with significant scatter in data. The grain size parameters d_{mli} and d_{ec} proved difficult to interpret and did not show any meaningful connection with fractional creep life exhaustion.

Carbide Phases, Composition, and Phase Equilibria

Ternary (FeCrV) composition diagram, BF-TEM images (same scale), and SAED pattern for M_3C, $M_{23}C_6$, M_7C_3, M_2C, and MC carbides present in 1CrMoV rotors are shown in Fig. 6. Each point on the ternary composition diagram shows the average carbide composition in the R and DSE states (bulk and peak stress) of rotors. The carbide phases observed in 1CrMoV rotors can be divided into five groups based on their composition and crystal structures: orthorhombic Fe-rich M_3C, cubic FeCr-rich $M_{23}C_6$, trigonal CrFe-rich M_7C_3, cubic V-rich MC, and hexagonal Mo-rich M_2C phases. The coarse platelike M_3C, fine spherical MC, very fine M_2C rods, and H-type (M_2C rods and spherical MC) carbides were observed in the R state. The peak stress area (DSE state) had various carbides, such as platelike M_3C, nondistinctive shaped M_2C, cube-shaped MC, H-type carbides, butterfly-shaped M_2C carbides, and nondistinctive shaped M_7C_3 and $M_{23}C_6$. The carbides in the DSE states were larger than those of the R state. No variations in carbide phases and morphology were noticed between the bulk and peak stress areas of the DSE states. In rotor 1, samples H3 and H4 exhibited consistent carbide phases and morphology.

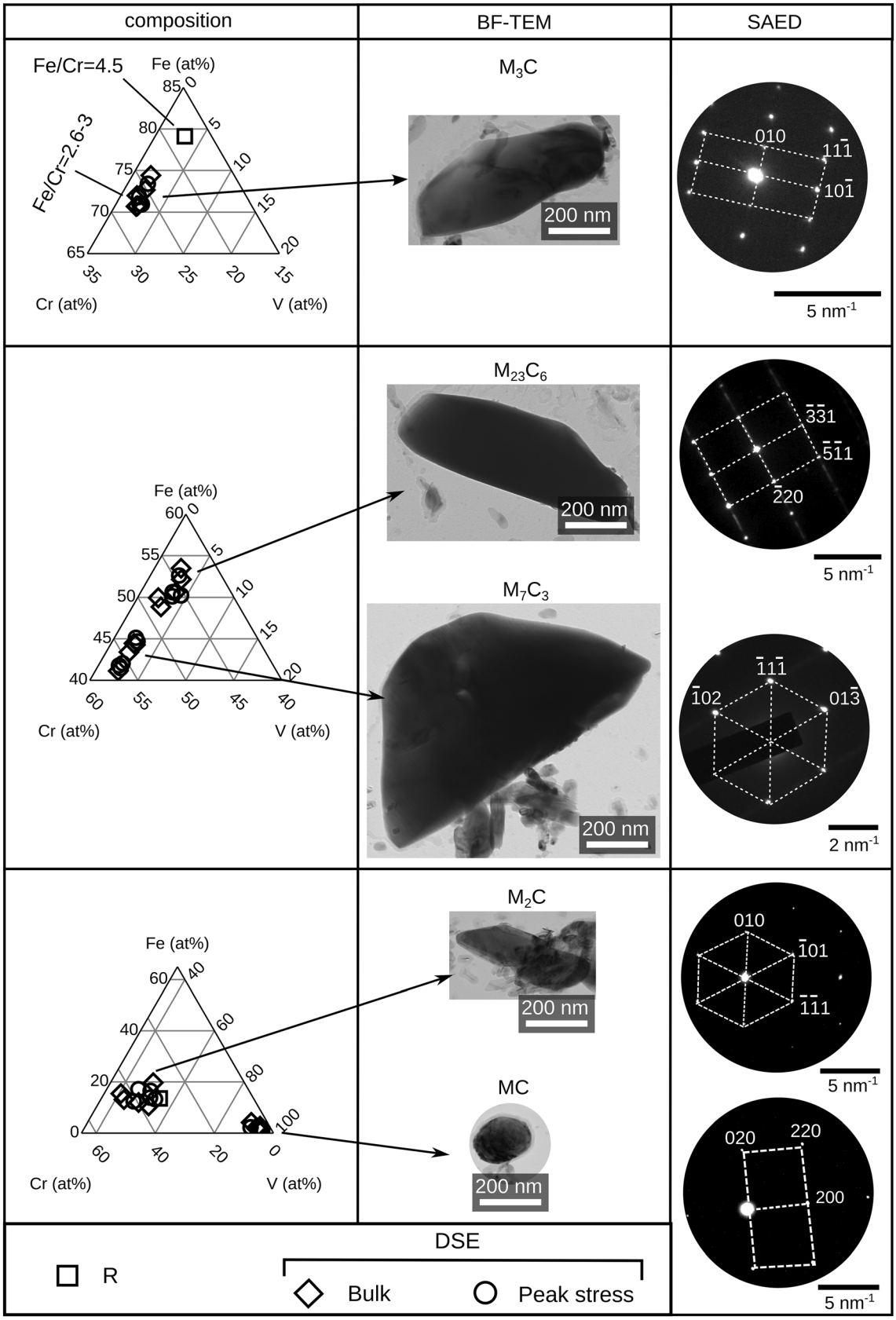
composition
BF-TEM
SAED
Fe/Cr=4.5
Fe (at%)
Fe/Cr=2.6-3
Cr (at%)
V (at%)
M3C
200 nm
010
111
101
5 nm-1
M23C6
331
511
220
M7C3
111
102
013
2 nm-1
M2C
010
101
111
MC
020
220
200
DSE
R
Bulk
Peak stress

◀**Fig. 6** FeCrV composition diagrams, BF-TEM images and SAED patterns for M_3C, $M_{23}C_6$, M_7C_3, M_2C, and MC carbides in R and DSE states of 1CrMoV rotors

EDX spot analysis showed that M_3C carbides in the peak stress areas (DSE state) had higher Cr and Mn contents compared to the R state. The Fe/Cr ratio in M_3C carbides experienced a decrease from ~ 4.5 (R state) to 3–2.6 in the peak stress area of the rotors (DSE state). The equilibrium composition of M_3C, as predicted by the ThermoCalc, had a lower Fe/Cr ratio of approximately 2. The composition of MC and M_2C carbides in the R and DSE states showed no significant differences. The compositional variations between the bulk and peak stress regions for each carbide phase were negligible. There were minimal compositional variations in rotor 1 between samples H3 and H4 for each carbide phase. The phase equilibrium in rotors 1 and 4 was predicted to comprise α-Fe, MC, and $M_{23}C_6$. The predicted phase equilibrium for rotors 2 and 3 included α-Fe, MC, $M_{23}C_6$, and M_7C_3.

Large areas of replicas containing many carbide precipitates (*overall carbides*) within a field of view (in TEM) were evaluated using EDX maps. Compared to the R state, the peak stress area (DSE state) exhibited notably higher levels of Cr and Mo, along with slightly elevated levels of Mn and V. In the R state, the Fe/Cr ratio was approximately 4.3, while in the peak stress area of the rotors, it varied from 1.1 to 1.7. The Fe/Mo ratio was approximately 9.4 in the R state, but ranged from 3.7 to 1.6 in the peak stress areas of the rotors. The Fe/Cr and Fe/Mo ratios were similar in both the bulk and peak stress regions of the DSE states. Similar Fe/Cr and Fe/Cr ratios were observed in Rotor 1 samples H3 and H4.

Carbide Parameters

TKD-EDX analysis (not shown) of the FIB samples extracted from the rotor 1 (H3) showed Fe-rich M_3C, CrFe-rich M_7C_3, and FeCr-rich $M_{23}C_6$ carbides on the grain boundaries. The V-rich MC and Mo-rich M_2C carbides were found on grain boundaries and within bainitic laths. TKD-EDX was used to study the carbide phases on extraction replicas. Figure 7 a and b compare TKD phase maps of extraction replicas from R and DSE states (bulk area) of rotor 1 (H3). Four areas within each region of interest were scanned by TKD, and the mean phase proportions for each area were calculated. The average phase proportion for each region of interest was computed by calculating the mean of means. Figure 7c shows the percentage phase proportions of carbide phases in the R state and peak stress area (DSE state) of the rotors. The M_3C was the main carbide in the R state of 1CrMoV rotor, only trace amounts of MC and M_2C were found. M_3C, M_2C, and M_7C_3 were the dominant carbide phases in the peak stress areas (DSE state) of the rotors, while MC and $M_{23}C_6$ were found in smaller amounts. The carbide phase proportions remained consistent in both the bulk and peak stress areas of the rotors. No significant differences in phase proportions were observed between the rotor 1 H3 and H4 DSE states (Fig. 7c).

The variation of (a) M_3C, (b) M_2C, and (c) M_7C_3 phase proportions with hardness-based fractional creep life exhaustion is shown in Fig 8. The error bars show the minimum and maximum average phase proportion of the four examined areas per region of interest. The error bars show the minimum and maximum phase proportion of the four examined areas per region of interest. As the creep life increased, M_3C proportions decreased while M_2C and M_7C_3 proportions increased. Fractional creep life showed a cubic correlation with the proportions of M_3C, M_2C, and M_7C_3 phases. There was a substantial spread in the data. The data obtained from rotor 4 (arrowed in Fig. 8) deviated from the observed trend. Fine carbides (~50 nm) such as MC and M_2C in the R state were not successfully indexed by the TKD technique. The TKD technique was ineffective at indexing thick sections of coarse M_2C, M_7C_3, and $M_{23}C_6$ carbides in the DSE states. Additional carbide parameters extracted from the TKD data included f_A, N_A, and λ_A. These parameters did not provide useful results for fractional creep life exhaustion due to the reasons explained later.

Discussion

Creep Life Assessment

The creep life exhaustion assessment was performed using conventional methods based on hardness (Table 1) and creep cavities (Table 2) measurements. The mean initial hardness of 1CrMoV rotor was 244 ± 7 HV which is within the range reported for 1CrMoV rotors in the pre-service condition [9, 12–14]. In the DSE state of all rotors, the hardness decreased due to creep exposure. The softening of 1CrMoV rotors at locations operated above 454 °C for more than 100 kh has been observed elsewhere [6–8, 12]. High localized stresses lead to creep cavitation on the peak stress region on the DSE state of 1CrMoV rotors. Creep cavitation damage in the blade attachment areas of retired rotors has been previously reported [1, 11].

In both hardness and cavitation creep life models, rotors 2 and 3 have higher fractional creep life exhaustion than rotors 1 and 4 regardless of operating time. Higher temperatures (T_e) lead to higher creep rates in rotors 2 and 3. The heterogeneity of PAG structure in 1CrMoV steel rotors

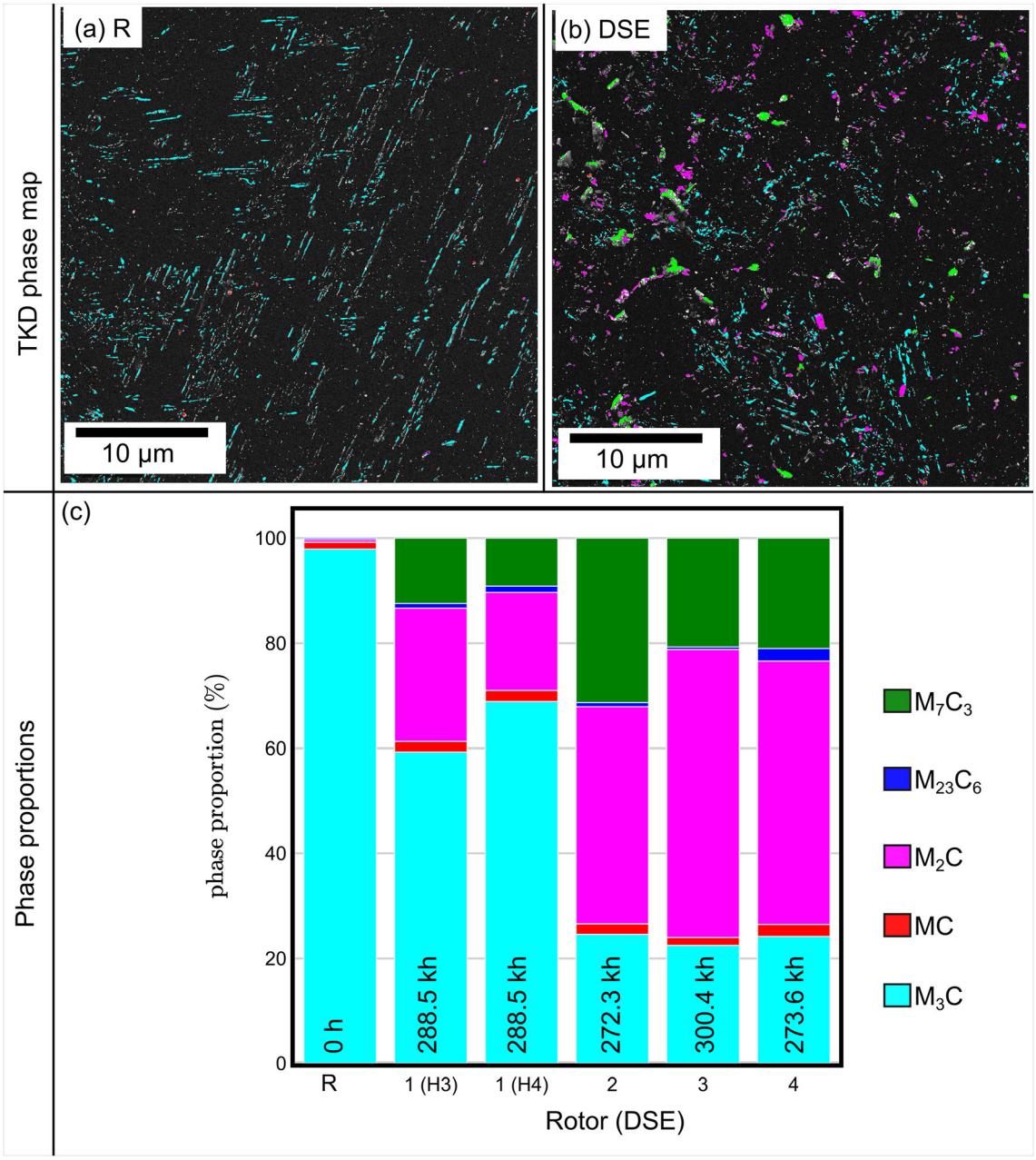

Fig. 7 Typical TKD phase map of carbides in the (**a**) R and (**b**) DSE of 1CrMoV rotors. (**c**) Carbide phase proportions (mean of means) in R and DSE states of the investigated rotors

does not influence hardness because rotor 1 samples H3 and H4 which have the same service history had similar hardness. This is consistent with Bhadeshia [5] who reported that hardness is not influenced by PAGs in bainite. However, cavitation-based creep life model produced different creep life values for two rotor 1 samples because of the differences observed in their PAG structure.

Microstructural Characterization

Several quantitative microscopy techniques were used in the current study. BSE and SE provide an overview of the general bainitic structure and creep cavitation over a large area. The observed bainitic structure comprising large and small grains and carbides is typical for 1CrMoV rotors [1, 24]. Using EBSD, the microstructural features of the bainitic structure were quantitatively analyzed, such as laths, packets, and PAGs. The bainitic structure observed by EBSD in the present study is consistent with that

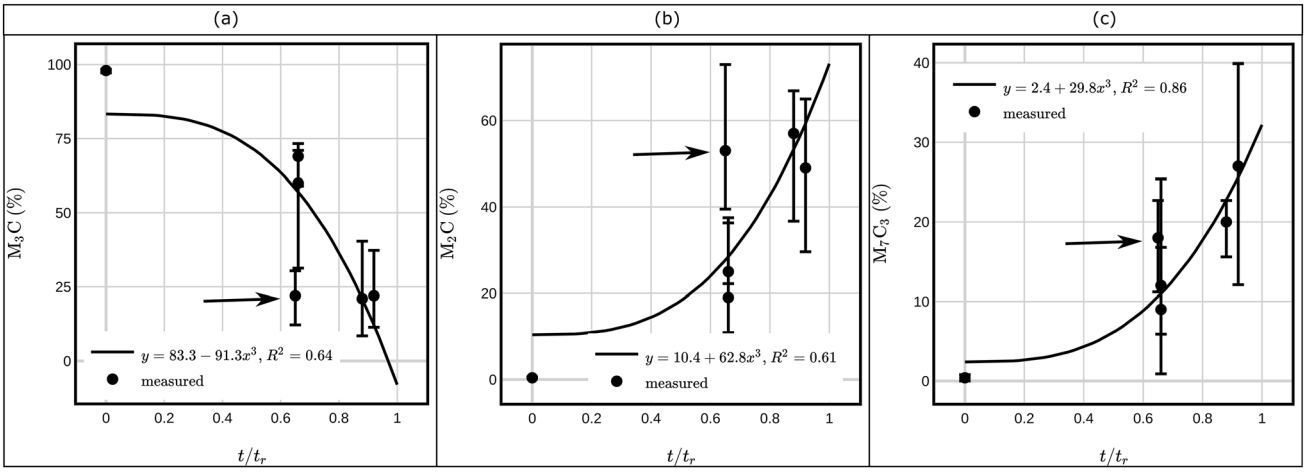

Fig. 8 Variation of (**a**) M_3C, (**b**) M_2C, and (**c**) M_7C_3 phase proportions (mean of means) with hardness-based creep life. (+error-max mean, -error-min mean)

reported by Ohtani et al. [25] on 1CrMoV steel. The grain structure of the investigated rotors is heterogeneous. The EBSD analysis of the R and DSE states did not show evidence of laths coarsening or PAGs refinement as the result of extended creep exposure. Previous studies reported coarsening of bainitic laths [9, 24, 25] in creep tested 1CrMoV steel and grain refinement [36] in 1CrMoV steel subjected to 540 °C. EBSD investigations reveal that cavity formation primarily occurs at PAG–PAG and PAG–lath boundary intersections. SE reveals that these intersections are sometimes accompanied by precipitates. The nucleation of creep voids on non-coherent precipitates on grain boundaries in 1CrMoV steels subjected to creep has been observed in other research [11, 62].

Few studies have combined quantitative STEM-EDX, TEM-SAED, and TKD analyses of carbides on extraction replicas and FIB lamella obtained from 1CrMoV rotors after prolonged service. In this study, a combined STEM-EDX, TEM-SAED, and TKD-EDS analyses performed on extraction replicas and FIB lamella identified to map out and obtained chemical composition of M_3C, MC, M_2C, M_7C_3, and $M_{23}C_6$ carbides present in 1CrMoV rotors. The structure of 1CrMoV steel rotors is upper bainite comprising Fe-rich M_3C, CrFe-rich M_7C_3, and FeCr-rich $M_{23}C_6$ on grain boundaries; V-rich MC and Mo-rich M_2C precipitates on grain boundaries and within bainitic ferrite matrix. The upper bainite structure and carbide phases in the pre-service and post-service conditions of 1CrMoV rotors observed in the current study are consistent with those in reference [7, 8, 23, 26]. The secondary precipitation of M_2C, M_7C_3, and $M_{23}C_6$ and coarsening of all carbide phases in the DSE states reported in the current study has been observed elsewhere [7, 8].

The chemical compositions of individual carbides and overall carbides on extraction replicas were extensively studied using STEM-EDX technique. In DSE states, during service at the T_e of ~ 529-548 °C, M_3C is chemically unstable in 1CrMoV rotors leading to the decrease of Fe/Cr in M_3C from ~ 4.5 to the range of 3–2.6 which is within the range of ± 2.8 reported elsewhere [8, 63]. The observed precipitation and coarsening of M_2C and M_7C_3 carbides in DSE states were accompanied by a decrease of Fe/Cr and Fe/Mo ratios in overall carbides due to service exposure. This decrease of Fe/Cr and Fe/Mo ratios in overall carbides in service-exposed 1CrMoV rotors has been reported by Mitchell and Moss [8]. The STEM-EDX procedure has a lateral resolution of the order of 10 nm and can reach a precision of ± 1 at.% [64]. The scatter in the average composition of each phase may be attributed to the variations in the composition of different rotors and composition of individual particles belonging to the same phase which varies with size and nucleation site.

The TKD technique allowed for identification carbides and measurements of parameters such as area fraction, diameter, interparticle spacing, number density, and phase proportions. Quantitative TKD analysis of carbide phase proportions showed that the R state comprises approximately 98% M_3C carbides, fine MC and M_2C existed as minority phases. Various authors [7, 8, 14, 23] reported similar carbide phases and their characteristics in the pre-service microstructure of 1CrMoV rotor steel. In the DSE state, the proportion of M_3C decreased significantly while M_2C and M_7C_3 increased and became the main carbide phases after service exposure which has been reported elsewhere [7, 8, 26]. The fine carbides could not be indexed successfully by TKD because 50 nm step size was too large [50, 51]. TKD technique did not index the thick parts of coarse carbides due to beam broadening [51]. The step size, thickness of carbides, and thickness of the carbon support affect the results obtained using the TKD technique.

Despite these limitations, the carbide phase proportions produced realistic results. No attempt was made in the current study to evaluate the evolution of the area fraction, number density, and interparticle spacing of carbides with service exposure because such measurements on extraction replicas depend on the extraction replica preparation.

The study examined the bulk and peak stress areas of 1CrMoV rotors to understand the influence of high localized stresses on microstructure and hardness over long-term service. The microstructural investigations conducted in this study revealed that there were no significant differences in volume-weighted average lath and PAG sizes, carbide phase proportions, carbide composition, and overall carbide composition results between bulk and peak stress regions. Hardness measurements showed that there were no significant differences between the bulk and peak stress areas in the DSE states. The high stresses in the peak stress area of the rotor disk did not cause noticeable changes in microstructure and hardness compared to the bulk area. The effect of stress on the softening of 1CrMoV rotor steels is significant only above ~ 108 MPa [18]. However, the effects of high localized stresses caused the local creep damage as cavities. The cavity density decreases in accordance with the stress gradient, which is the highest at the T-corner.

Microstructural Evolution with Creep Life

Bainitic Laths

The bainitic lath size (Fig. 5a) and surface density (Fig. 5b) showed a good correlation with the fractional creep life exhaustion, but the grain structure heterogeneity introduced a large scatter in these parameters. Previous studies reported coarsening of bainitic laths with strain and fractional creep life exhaustion in creep tested 1CrMoV steel [9, 24, 25]. However, grain refinement has been reported for 1Cr0.25Mo0.25V steel main steam pipeline operated for ~ 200 kh at ~ 540 °C and ~ 70 MPa [36]. The finer grain structure in rotor 1 H3 had more nucleation sites for cavities compared to the coarser grain structure of H4. This difference explains the inconsistency in the estimated fractional creep life exhaustion of rotor 1. The grain structure heterogeneity across the rotor impacts the estimated fractional creep life exhaustion calculated using the creep cavitation model. It is unclear whether creep exposure or initial grain structure characteristics are responsible for the variation in lath d_V or S_V with creep life exhaustion.

Carbide Phase Proportions

The phase proportions of M_3C, M_2C, and M_7C_3 carbides had a good correlation with the hardness-based creep life exhaustion, with scatter in the data. This scatter is caused by the uneven distribution of carbides in the 1CrMoV steel rotor and inability of the TKD technique to map the coarse carbides. The proportion of M_3C carbides in 1CrMoV rotor decreases with a simultaneous increase of M_2C and M_7C_3 carbides as creep progresses during service at higher temperatures. Dobrzanski et al. [65] related the creep life exhaustion of 1Cr0.5Mo low-alloy steel after long-term creep to the changes in carbide types and their quantitative fractions. They reported a decrease in the percentage fraction of M_3C with creep life exhaustion. This study found that M_3C carbides exist in the R state of a 1CrMoV rotor in measurable sizes. This means their changes can be tracked during service and potentially used to predict the creep life exhaustion of 1CrMoV steel rotors. Once the dissolution of M_3C is complete, the evolution of a more stable M_2C phase has a potential to be used for life assessment. TKD data for rotor 4 (marked by an arrow in Fig. 8) showed that the hardness-based creep life model underestimated the creep life exhaustion, as the microstructure was severely degraded. This suggests that TKD analysis of carbides can improve the accuracy of creep life models.

Microstructure-Based Creep Life Assessment

The current study found the quantitative relationship between the microstructure and creep life exhaustion in four service-exposed 1CrMoV rotors. However, a precise correlation between microstructural parameters and creep life exhaustion requires extensive experimental data from many service-exposed rotors. The scope of this work focused on four rotors only, but future work will incorporate experimental data from the remaining six service-exposed rotors, which can be time consuming. The microstructural heterogeneity across the rotor can also make it difficult to accurately interpret microstructural parameters like bainitic lath size. The heterogeneity did not have a major impact on the proportions of the carbide phases, making it the most effective technique for estimating creep life. The TKD technique proved to be the good technique for the identification and mapping of carbides phases. Proper identification and mapping of carbides with the TKD technique rely on the quality of the diffraction pattern, which depends on the thickness of the carbide. Future TKD carbide examinations will be enhanced by combining dictionary indexing with EDX.

Conclusions

The potential of electron microscopy techniques as a tool for assessing the life of long-term service-exposed 1CrMoV steel rotors base on the microstructure was explored. This was done by examining different microstructural features using electron microscopy and analyzing their correlation with fractional creep life exhaustion based on hardness and cavitation. The conclusions can be summarized as follows:

- The hardness for the rotors decreased during the long-term service. The hardness and estimated creep life exhaustion, determined by hardness, are not affected by the microstructural heterogeneity across the rotor.
- The cavities developed in the highest stressed areas of the rotors during service. The grain structure heterogeneity on the rotor has implications for both the measured cavity parameters, and the estimated creep life exhaustion based on cavities.
- The bainitic lath volume-weighted average size and surface density correlated with fractional creep life exhaustion estimated based on cavities. The grain structure heterogeneity prevents the effective use of bainitic laths for creep life assessment based on microstructure.
- The proportions of M_3C, M_2C, and M_7C_3 carbides correlated with the creep life exhaustion estimated based on hardness. The proportions of the carbide phases were found to be the most effective in evaluating creep life using a microstructure. However, the evolution of carbide proportions does not offer a means to predict creep crack initiation.
- The high stress in the peak stress regions of the stage 1 disk did not noticeably impact microstructural parameters and hardness. However, stress had a notable impact on creep cavitation.
- BSE-SEM, EBSD-EDX, and TKD-EDX are suitable techniques for quantitative analysis of cavities, bainitic laths, and carbides, respectively.

Acknowledgments HSN and JEW acknowledge the financial support of the National Research Foundation of South Africa (Grant Number 70724) and ESKOM through the Eskom Power Plant Engineering Institute (EPPEI).

Authors Contribution HSN conceptualized the project, collected microstructural data, conducted quantitative data analysis, and wrote the manuscript. JEW conceptualized the project, collected microstructural data, and edited the manuscript. RK edited the manuscript. All authors reviewed and edited the original draft, discussed the results, and contributed to writing the manuscript.

Funding Open access funding provided by Nelson Mandela University.

Data Availability Data will be made available on request.

Conflict of interest The authors declare that they have no known competing financial interests or personal relationships that could have appeared to influence the work reported in this paper.

Open Access This article is licensed under a Creative Commons Attribution 4.0 International License, which permits use, sharing, adaptation, distribution and reproduction in any medium or format, as long as you give appropriate credit to the original author(s) and the source, provide a link to the Creative Commons licence, and indicate if changes were made. The images or other third party material in this article are included in the article's Creative Commons licence, unless indicated otherwise in a credit line to the material. If material is not included in the article's Creative Commons licence and your intended use is not permitted by statutory regulation or exceeds the permitted use, you will need to obtain permission directly from the copyright holder. To view a copy of this licence, visit http://creativecommons.org/licenses/by/4.0/.

References

1. Metallurgical Guidebook for Steam Turbine Rotors and Discs, Volume 1 Chemistry, manufacturing, service degradation, life assessment, and repair, EPRI, Palo Alto, 2009.
2. P. van der Meer, B. Sonderegger, J.E. Westraadt, M.E.J. Bezuidenhout, Effect of geometry on the microstructural ageing of a 1CrMoNiV turbine rotor steel, in International ECCC conference, 2014.
3. F.H. van Zyl, G. Von dem Bongart, M.E.J. Bezuidenhout, P. Doubell, F.C. Havinga, D.A.H. Pegler, W. Smit, Life assessment and creep damage monitoring of high temperature pressure components in South Africa's power plant, in ECCC Creep Conference, London, UK, 2005, pp. 12–14.
4. P. Doubell, R. Scheepers, M. Newby, D.G. Hattingh, L. Von Wielligh, D. Odendaal, I.N. Weddeburn, novel core sampling technique for hp turbine rotor remaining life study, in Tenth International EPRI Welding & Repair Technology Conference, Island, 2012.
5. H.K.D.H. Bhadeshia, *Bainite in steels: theory and practice*, 3rd edn. (CRC Press, 2019)
6. N.S. Cheruvu, Degradation of mechanical properties of Cr-Mo-V and 2.25Cr-1Mo steel components after long-term service at elevated temperatures. Metall. Trans. A. **20**, 87–97 (1989)
7. A. Joarder, D.S. Sarma, N.S. Cheruvu, Effect of long-term service exposure on microstructure and mechanical properties of a CrMoV steam turbine rotor steel. Metall. Trans. A. **22**, 1811–1820 (1991)
8. D.R.G. Mitchell, C.J. Moss, Characterization of seven power-generating turbine rotors using microscopy-based techniques. J. Mater. Eng. Perform. **7**, 621–631 (1998)
9. N. Shinya, J. Kyono, H. Kushima, Creep fracture mechanism map and creep damage of Cr–Mo–V turbine rotor steel. ISIJ Int. **46**, 1516–1522 (2006)
10. H.K.D.H. Bhadeshia, A. Strang, D.J. Gooch, Ferritic power plant steels: remanent life assessment and approach to equilibrium. Int. Mater. Rev. **43**, 45–69 (1998)
11. R. Viswanathan, *Damage mechanisms and life assessment of high temperature components*. (ASM International, 1989)
12. B.R. Cardoso, C.F.T. Matt, H.C. Furtado, L.H. de Almeida, Creep damage evaluation in high-pressure rotor based on hardness measurement. J. Mater. Eng. Perform. **24**, 2784–2791 (2015)

13. V.P. Swaminathan, R. Viswanathan, C.P. Clark, Material property studies of two high-pressure turbine rotors for remaining life assessment. J. Eng. Mater. Technol. **116**, 19–26 (1994)
14. L. Binda, *Advanced creep damage and deformation assessment of materials subject to steady and cyclic loading conditions at high temperatures*. (ETH Zurich, 2010)
15. Q. Zhe, S. Fu, C.J. McMahon Jr., *Temper embrittlement of CrMoV turbine-rotor steels*. (Univesity of Pennysylvania, Philadelphia, 1982)
16. T. Goto, Study on residual creep life estimation using nondestructive material properties tests, in International Conference on Creep and Fracture of Engineering Materials and Structures, Pineridge Press, Swansea, UK, 1984, pp. 1135.
17. D.J. Gooch, *Remnant creep life prediction in ferritic materials*. (Elsevier, 2003)
18. A.D. Batte, D.J. Gooch, Metallurgical aspects of remanent life assessment of high temperature rotor forgings, life assessment and improvement of turbo-generator rotors for fossil plants, (1984) 3.
19. A. Raj, N. Roy, B.N. Roy, A.K. Ray, Life estimation and creep damage quantification of service exposed reformer tube. High Temp. Mater. Process. **34**, 731–742 (2015)
20. T. Sumida, T. Ikuno, M. Sukekawa, Weibull distribution of the cavity length during creep in a Cr-Mo-V steel. J. Mater. Sci. Lett. **13**, 1625–1628 (1994)
21. J.D. Parker, Creep cavitation in CSEF steels, in Seventh International Conference Advances in Materials Technology for Fossil Power Plant, 2013, pp. 714.
22. J. Ewald, C. Berger, K.-H. Keienburg, W. Wiemann, Present quality level of large heat resistant rotor forgings made of 1%CrMoV steels–Part 1. Steel Res. **57**, 83–92 (1986)
23. T.H. Lee, C.S. Oh, S.H. Ryu, J.T. Kim, Crystallography and morphology of carbides in a low-cycle fatigued 1Cr-1Mo-0.25V steel. Metall. Mater. Trans. A. **42**, 147–157 (2011)
24. T. Ohtani, H. Ogi, M. Hirao, Evolution of microstructure and acoustic damping during creep of a Cr–Mo–V ferritic steel. Acta Mater. Mater. **54**, 2705–2713 (2006)
25. T. Ohtani, F. Yin, Y. Kamada, Creep-induced microstructural changes and acoustic characterization in a Cr–Mo–V Steel. Jpn. J. Appl. Phys.. J. Appl. Phys. **47**, 3916 (2008)
26. B.A. Senior, A critical review of precipitation behaviour in 1Cr-Mo-V rotor steels. Mater. Sci. Eng. A. **103**, 263–271 (1988)
27. H.G.A. Bates, K.A. Ridal, *Factors governing the creep properties in large diameter 1 per cent chromium-molybdenum-vanadium rotor forgings* (Institution of Mechanical Engineers, 1963), p.99–113
28. S.C. Bose, K.S. Reddy, G. Reddy, K. Singh, D.S. Sarma, Effect of service-simulated aging on the microstructure and properties of casing casting steel (1CrMoV) vis-à-vis remnant life assessment. Metall. Mater. Trans. A. **34**, 1265–1274 (2003)
29. G.L. Dunlop, R.W.K. Honeycombe, Ferrite morphologies and carbide precipitation in a Cr-Mo-V creep-resisting steel, Metal. Science. **10**, 124–132 (1976)
30. X. He, C. Hu, Z. Wang, H. Zhao, X. Wei, H. Dong, Carbide transformation behaviors of a Cr–Mo–V secondary hardening steel during over-ageing. Mater. Res. Express. **7**, 036511 (2020)
31. J. Janovec, A. Kroupa, M. Svoboda, A. Vy'Rostková, H.J. Grabke, Evolution of secondary phases in Cr-V and Cr-Mo-V low alloy steels. Can. Metall. Q. **44**, 219–232 (2005)
32. Z. Liu, C. Liu, L. Miao, X. Guo, J. Ding, H. Zhang, The evolution of complex carbide precipitates in a low alloy Cr–Mo–V steel after long-Term aging treatment. Materials. **12**, 1724 (2019)
33. A. Výrostková, A. Kroupa, J. Janovec, M. Svoboda, Carbide reactions and phase equilibria in low alloy Cr–Mo–V steels tempered at 773–993 K part I: experimental measurements. Acta Mater. Mater. **46**, 31–38 (1998)
34. Z. Yongtao, M. Lede, W. Xiaojun, Z. Hanqian, L. Jinfu, Evolution behavior of carbides in 2.25 Cr-1Mo-0.25 V steel. Mater. Trans. **50**, 2507–2511 (2009)
35. Y. Zhang, P. Luo, H. Yan, H. Zhang, J. Li, The effect of bainite type on the evolution of carbide constituent during an accelerated aging in Cr-Mo-V steel. J. Mater. Eng. Perform. **28**, 578–585 (2019)
36. G. Bakic, V. Sijacki Zeravcic, M. Djukic, V. Maksimovic, B. Rajicic, Material characterization of 1Cr0.25Mo0.25V power plant steel after prolonged service, First Metallurgical & Materials Engineering Congress of South-East Europe, Belgrade, Serbia, 2013, pp. 380–387.
37. J. Dong, Y. He, G. Song, J. Jung, K. Shin, Evolution of carbide morphology and composition in Cr–Mo–V steel after service exposure. Mater. Technol. **27**, 70–72 (2012)
38. G. Golański, P. Wieczorek, Precipitation of carbides in Cr-Mo-V cast steel after service and regenerative heat treatment, Arch. Found. Eng. 9 (2009).
39. M. Kvapilová, M. Ohanková, P. Král, J. Dvořák, K. Kuchařová, J. Čmakal, V. Sklenička, Characterization of creep properties and the microstructure of a service-exposed low alloy CrMoV steel steam pipe. Mater. Sci. Eng. A. **853**, 143684 (2022)
40. A. Zieliński, J. Dobrzański, T. Jóźwik, Assessment of loss in life time of the primary steam pipeline material after long-term service under creep conditions. J. Achiev. Mater. Manuf. Eng. **54**, 67–74 (2012)
41. A. Zieliński, J. Dobrzański, H. Krztoń, Structural changes in low alloy cast steel Cr-Mo-V after long time creep service. J. Achiev. Mater. Manuf. Eng. **25**, 33–36 (2007)
42. R. Singh, S. Banerjee, Morphological and compositional changes of the carbides in Cr-Mo-V ferritic steel. Mater. Sci. Eng. A. **132**, 203–211 (1991)
43. H.R. Tipler, B.E. Hopkins, The creep cavitation of commercial and high-purity Cr-Mo-V steels. Metal. Sci. **10**, 47–56 (1976)
44. N. Bandyopadhyay, C.L. Briant, E.L. Hall, Carbide precipitation, grain boundary segregation, and temper embrittlement in NiCrMoV rotor steels. Metall. Trans. A. **16**, 721–737 (1985)
45. D. Lonsdale, P.E.J. Flewitt, Damage accumulation and microstructural changes occurring during the creep of a 2.14% Cr1% Mo steel. Mater. Sci. Eng. **39**, 217–229 (1979)
46. R.A. Stevens, P.E.J. Flewitt, Recovery of creep properties of a vanadium-strengthened steel (1Cr1Mo0.75VTiB) by reheat treatment. Metall. Trans. A. **15**, 707–718 (1984)
47. S.H. He, B.B. He, K.Y. Zhu, M.X. Huang, On the correlation among dislocation density, lath thickness and yield stress of bainite. Acta Mater. Mater. **135**, 382–389 (2017)
48. A. Zieliński, J. Dobrzański, G. Golański, Estimation of the residual life of L17HMF cast steel elements after long-term service. J. Achiev. Mater. Manuf. Eng. **34**, 137–144 (2009)
49. H. Wang, A. Kostka, W.E. Goosen, G. Eggeler, J.E. Westraadt, TEM replica analysis of particle phases in a tempered martensite ferritic Cr steel after long term creep. Mater CharactCharact. **181**, 111–396 (2021)
50. J.E. Westraadt, W.E. Goosen, A. Kostka, H. Wang, G. Eggeler, Modified Z-phase formation in a 12%Cr tempered martensite ferritic steel during long-term creep. Mater. Sci. Eng. A. **855**, 143857 (2022)
51. A. Bhattacharya, C. Parish, J. Henry, Y. Katoh, High throughput crystal structure and composition mapping of crystalline nanoprecipitates in alloys by transmission Kikuchi diffraction and analytical electron microscopy. Ultramicroscopy. **202**, 33–43 (2019)
52. H.S. Nyembe, J.E. Westraadt, *Microstructural based creep life assessment of 1CrMoV turbine rotor steels after long-term service, physics*. (Nelson Mandela University, 2023)

53. T. Goto, Microstructure and mechanical properties of ageing materials, ASM Fall Meeting, Chicago, IL, (1992).
54. F. Niessen, T. Nyyssönen, A. Gazder, R. Hielscher, Parent grain reconstruction from partially or fully transformed microstructures in MTEX. J. Appl. Crystallogr.Crystallogr. **55**, 180–194 (2022)
55. R. Hielscher, T. Nyyssönen, F. Niessen, A. Gazder, The variant graph approach to improved parent grain reconstruction. Materialia. **22**, 101399 (2022)
56. MATLAB, The MathWorks Inc., Natick, Massachusetts, (2019).
57. F. Bachmann, R. Hielscher, H. Schaeben, *Texture analysis with MTEX–free and open source software toolbox, solid state phenomena* (Trans Tech Publ, 2010), p.63–68
58. P. Lehto, H. Remes, T. Saukkonen, H. Hänninen, J. Romanoff, Influence of grain size distribution on the Hall-Petch relationship of welded structural steel. Mater. Sci. Eng. A. **592**, 28–39 (2014)
59. P. Stadelmann, JEMS JAVA electron microscopy software, (2012).
60. J.O. Andersson, T. Helander, L. Höglund, P. Shi, B. Sundman, Thermo-Calc & DICTRA, computational tools for materials science. Calphad. **26**, 273–312 (2002)
61. J.M. Sosa, D.E. Huber, B. Welk, H.L. Fraser, Development and application of MIPAR^{TM}: a novel software package for two-and three-dimensional microstructural characterization. Integr. Mater. Manuf. Innov. **3**, 123–140 (2014)
62. K. Yamagiwa, T. Hiramatsu, S. Kataoka, S. Izumi, S. Sakai, Quantitative analysis of three-dimensional geometry of creep void observed in 1Cr-1Mo-0.25 V turbine rotor steel, in International Conference on Advanced Technology in Experimental Mechanics, The Japan Society of Mechanical Engineers, (2011).
63. J. Maguire, D.J. Gooch, Metallographic techniques for residual life assessment of 1CrMoV rotor forgings, in International Conference on Life Assessment and Extension, (1988), p. 116–124.
64. B. Carter, D. Williams, *Transmission electron microscopy: diffraction, imaging, and spectrometry*. (Springer, 2016)
65. J. Dobrzański, H. Krztoń, A. Zieliński, Development of the precipitation processes in low-alloy Cr-Mo type steel for evolution of the material state after exceeding the assessed lifetime. J. Achiev. Mater. Manuf. Eng. **23**, 19–22 (2007)

Publisher's Note Springer Nature remains neutral with regard to jurisdictional claims in published maps and institutional affiliations.